Journal of the Mechanics and Physics of Solids 112 (2018) 253–272

Contents lists available at ScienceDirect

Journal of the Mechanics and Physics of Solids

journal homepage: www.elsevier.com/locate/jmps

Mixing by shear, dilation, swap, and diffusion

Laurence Brassart[a,*], Qihan Liu[b], Zhigang Suo[b]

[a] Department of Materials Science and Engineering, Monash University, Clayton, VIC, 3800, Australia
[b] School of Engineering and Applied Sciences, Kavli Institute for Bionano Science and Technology, Harvard University, Cambridge, Massachusetts, 02138, USA

ARTICLE INFO

Article history:
Received 8 November 2017
Revised 18 December 2017
Accepted 18 December 2017
Available online 19 December 2017

Keywords:
Interdiffusion
Creep
Supercooled liquids
Glasses
Gels

ABSTRACT

This paper presents a theory of poroviscosity for binary solutions. Subject to mechanical forces and connected to reservoirs of molecules, a binary solution evolves by concurrent flow and diffusion. Our theory generalizes the classical theory of interdiffusion by decoupling the molecular processes for flow and diffusion. We further remove the assumption of local chemical equilibrium, so that the insertion of molecular into a material element, accompanied by a change in volume, is treated as non-equilibrium process and is put on the same footing as the process of shear deformation by viscous flow. The theory of poroviscosity has an intrinsic length scale, called the poroviscous length, below which the homogenization of a composition heterogeneity is limited by viscous flow, rather than by diffusion. The theory has implications for the analysis of interdiffusion in systems that display a decoupling between flow and diffusion, such as supercooled liquids, glasses, and physical gels. We illustrate the theory with numerical examples of a layered structure and a spherical particle. We discuss the results for feature sizes below and above the poroviscous length.

1. Introduction

Diffusion and flow in liquids and solids require molecules to change neighbors. Diffusion refers to the migration of a particle relative to its surrounding molecules, and the diffusivity D characterizes the rate of diffusion. Flow refers to the molecular motion to relax an applied stress, and the viscosity η gives the proportionality ratio between the stress and strain rate. Einstein (1905) assumed that a particle diffuses in a liquid by the Stokes creep of the liquid, and related the diffusivity D of the particle to the viscosity η of the liquid:

$$\frac{D\eta}{kT} = \frac{1}{Ca} \tag{1}$$

where k is Boltzmann constant, T is the temperature, a is a length of the order of the size of the particle, and C is a dimensionless number. Einstein derived this relation for a diffusing particle much larger than the molecules of the surrounding liquid, but the relation holds remarkably well for particles of sizes down to that of the molecules of the surrounding liquid, including self-diffusion (Edward, 1970). For a particle diffusing in a viscous liquid, the Stokes-Einstein relation holds because both the diffusion of the particle and the flow of the liquid are rate-limited by a single molecular process: molecules of the liquid change neighbors.

* Corresponding author.
E-mail address: laurence.brassart@monash.edu (L. Brassart).

https://doi.org/10.1016/j.jmps.2017.12.008
0022-5096/

The Stokes-Einstein relation, however, fails in most materials. The failure simply indicates that more than a single molecular process mediates diffusion and flow. For example, in a physically crosslinked gel, flow requires the breaking and reforming of the physical crosslinked network, whereas diffusion of the solvent can happen through the mesh of the polymer without rearranging the network (Phillips et al., 1989). As a second example, at a low temperature, flow of a crystalline solid is often mediated by dislocations, and is unrelated to self-diffusion. At a high temperature, flow of a crystalline solid can be mediated by self-diffusion, but the viscosity also depends on the grain size, as in the Herring creep (Herring, 1950) and the Coble creep (Coble, 1963). As a third example, in a supercooled liquid, molecules form a dynamically heterogeneous structure. Molecules move fast in some regions and slow in others (Berthier, 2011; Ediger, 2000; Karmakar et al., 2014). Flow requires the rearranging of the slow moving regions, but diffusion can be facilitated by molecules hopping in the fast moving regions (Li et al., 2014; Liu et al., 2015).

This paper formulates a continuum theory of coupled flow and diffusion in a solution of two species of molecules. We view the solution as a body of many small pieces. Each piece consists of many molecules and evolves through a sequence of homogeneous states. Different pieces communicate through the compatibility of deformation, conservation of molecules, and balance of forces. For a homogeneous solution of fixed numbers of both species of molecules, the volume of the solution is taken to be independent of stress. We call such an idealized solution a molecularly incompressible solution. In our previous work (Brassart et al., 2016), we have identified that the homogeneous state of a molecularly incompressible solution of two molecular species can evolve in three modes: shear, dilation, and swap.

- Shear changes the shape of a piece, but preserves the number of each species of molecules in the piece.
- Dilation changes the volume of a piece by inserting molecules into, or removing molecules from, the piece, but preserves the ratio of the two species of molecules and the shape of the piece.
- Swap changes the ratio of the two species of molecules, but preserves both the shape and volume of the piece.

The shape, volume, and composition evolve when a piece of homogeneous binary solution is subject to a combination of mechanical and chemical loads. All three modes break and form intermolecular bonds. We place the three modes on equal footing, as distinct, concurrent, non-equilibrium processes. Our theory thus removes the bias that assumes local chemical equilibrium but allows the non-equilibrium process of shear. Specifically, we do not assume chemical equilibrium at the scale of the individual piece. While diffusion is assumed as infinitely fast at the scale of a single piece, change in composition by insertion and removal of species (leading to dilation or swap) may take time. The apparent paradox is resolved by recalling the presence of fast diffusion paths that allow the fast redistribution of species across the piece.

The relaxation of the local chemical equilibrium is a fundamental departure from most the classical thermodynamic theory of irreversible processes (de Groot and Mazur, 1984). The idea was first proposed by Brassart and Suo (2012, 2013) in the context of chemically reactive host-guest systems. In our previous work (Brassart et al., 2016), we presented a thermodynamic theory of mixing in a body small enough so that diffusion is taken to be infinitely fast. We now generalize our theory into a theory that couples flow and diffusion. We also discuss the implementation of the theory using the finite element method.

To focus on the essential idea of coupled diffusion and flow without assuming local chemical equilibrium, here we neglect elasticity. Elasticity is obviously important in solids, but including elasticity here will obscure the coupling between diffusion and the three local non-equilibrium processes, shear, dilation and swap. The coupling between elasticity, flow and diffusion will be addressed elsewhere. Also see a coupled theory of viscoelasticity and poroelasticity (Hu and Suo, 2012).

Continuum mechanics describes deformation of a body by the movements of material particles. Such a description assumes that each material particle is a piece of the material with a fixed identity and number of molecules - that is, each piece is a closed thermodynamic system. However, the notion of material particles is unsuitable when all molecules can diffuse, because small pieces of material no longer preserve the identity and number of molecules in time - that is, each small piece is an open thermodynamic system. Following Darken (1948), we imagine markers dispersed in the body, such as those used to visualize the flow in hydrodynamic and metallurgical experiments. The markers are inert particles, and do not react with the molecules of the body. An individual marker is small enough to be carried with the flow without perturbing it, but is large enough to diffuse negligibly. We track the flow in the body by the movements of the markers, and identify the diffusion flux of each species of molecules by the flux relative to the markers. In effect, we use the markers to label small pieces of materials. Thus, the notion of markers replaces the conventional notion of material particles. As we will demonstrate below, with some care in interpretation, most equations in conventional continuum mechanics are applicable for markers.

Our theory based on markers differs from the classical Navier-Stokes equations for solutions, which is based on the barycentric velocity and does not allow for independent diffusion fluxes of the two species (de Groot and Mazur, 1984; Landau and Lifshitz, 1987). Our theory is also distinct from that due to Darken (1948) and Stephenson (1988), who assumed local chemical equilibrium. Darken (1948) only considered a special case that flow is so fast that the motion of the markers is limited by the diffusion of molecules. In the case of single species, our theory is consistent with the theory for coupled creep and self-diffusion (Li et al., 2014; Pharr et al., 2011; Suo, 2004). Our theory based on markers also differs from the theory coupling diffusion and creep in a crystal, which uses a crystalline lattice to label material particles (Fischer and Svoboda, 2014; Larché and Cahn, 1985; Mishin et al., 2013; Villani et al., 2015). Our theory also differs from the theory of coupled diffusion and deformation in a gel, which uses a covalent polymer network to label material particles

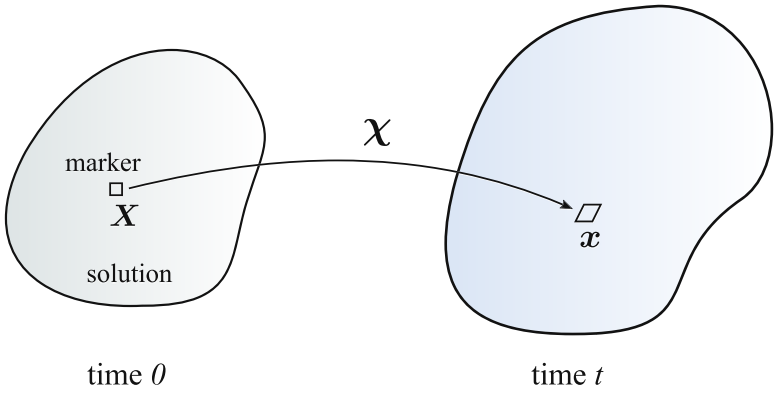

Fig. 1. A body of a binary solution evolves through a sequence of inhomogeneous configurations by flow and diffusion. The coordinate of a marker is $\boldsymbol{X}$ at time 0, and is $\boldsymbol{x}$ at time t.

(Bouklas et al., 2015; Chester and Anand, 2010; Drozdov and Christiansen, 2013; Hong et al., 2008). Analogous to Biot's theory of poroelasticity (Biot, 1941), the theory developed in this paper may be called poroviscosity.

Like other theories of coupled diffusion and creep, our theory of poroviscosity specifies a length, which we call the poroviscous length:

$$\Lambda = \sqrt{\frac{D\eta V}{kT}}, \tag{2}$$

where V is a volume characteristic of the molecular volume. The poroviscous length represents the length scale where diffusional relaxation and viscous relaxation happen at comparable rate. When the size of a composition heterogeneity is small relative to the poroviscous length, homogenization is limited by viscous flow, rather than by diffusion. In our theory, this is also true in the absence of any applied stress. When the size of a composition heterogeneity is large relative to the poroviscous length, homogenization is limited by diffusion. This is the case when the Stokes–Einstein relation (1) holds, and the poroviscous length is of the order of the molecular size. Our theory then recovers the theory due to Stephenson (1988). Section 2 formulates the theory of poroviscosity for binary solutions within a thermodynamically-consistent and Lagrangian setting. Specific forms of the free energy function and kinetic models are given in Section 3. Boundary-value problems are discussed in Section 4, and a numerical implementation based on the finite element method is outlined in Section 5. In Section 6 we illustrate the theory in two examples: interdiffusion in a binary couple and swelling of a particle. Appendix A formulates the theory in an Eulerian setting and compares the theory to the Navier–Stokes equations. An analytical solution to the linearized 1D interdiffusion problem is presented in Appendix B.

2. Theory of poroviscosity

We develop poroviscosity of binary solutions; extension to solutions of more than two molecular species should not cause conceptual difficulty. Two species of molecules, A and B, are taken to be miscible in any proportion to form a solution. Subject to a history of mechanical and chemical loads, a body of the solution flows, and its composition varies in space and time (Fig. 1). Imagine markers dispersed in the body. Associated with a marker is a small piece of the solution. Each individual piece evolves through a sequence of homogeneous states by shear, dilation, and swap. Different pieces communicate through the compatibility of deformation, conservation of molecules, and balance of forces. We now develop a continuum theory that evolves the coordinates of the markers, as well as the compositions of the small pieces.

2.1. Compatibility of deformation

Let the coordinate of a marker be $\boldsymbol{X}$ at time 0, and be $\boldsymbol{x}$ at time t. The motion map

$$\boldsymbol{x} = \boldsymbol{\chi}(\boldsymbol{X}, t) \tag{3}$$

describes the trajectory of the marker. The velocity of the marker is $\boldsymbol{v} = \partial\boldsymbol{\chi}(\boldsymbol{X}, t)/\partial t = \dot{\boldsymbol{\chi}}$. In the absence of diffusion, the continuity of the motion map (3) requires that markers located on the surface of the body at time 0 remain on the surface of the body at all subsequent times (Mandel, 1966). We assume that this is still the case in the presence of diffusion of the molecules. This assumption means that molecules in the environment do not plate onto the external surface, but diffuse into the bulk of the body.

The motion of markers relative to each other describes the deformation of the solution through the deformation gradient

$$\boldsymbol{F} = \nabla\boldsymbol{\chi}, \tag{4}$$

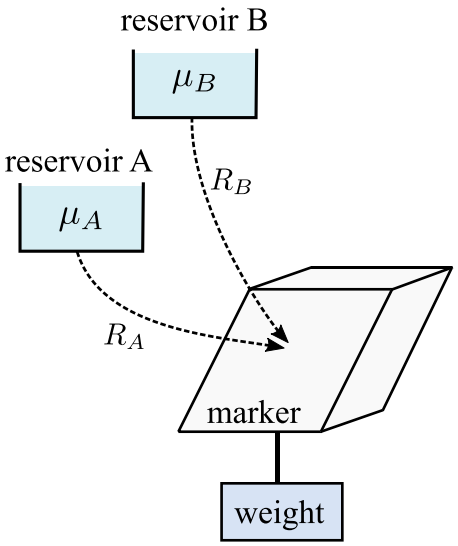

Fig. 2. A binary solution of species A and B is subject to mechanical and chemical loads. Associate each small piece of the body to a marker. Represent a mechanical load by connecting the small piece to a hanging weight. Represent chemical loads by connecting the small piece to reservoirs of species A and B with prescribed chemical potentials.

where ∇ represents the gradient with respect to the coordinates $\boldsymbol{X}$ of the markers in the reference configuration. We also introduce the spatial velocity gradient, $\boldsymbol{L} = grad(\boldsymbol{v}) = \dot{\boldsymbol{F}}\boldsymbol{F}^{-1}$, where $grad(\cdot)$ represents the gradient with respect to the coordinates $\boldsymbol{x}$ of the markers in the deformed configuration. The rate of deformation is defined as the symmetric part of the spatial velocity gradient:

$$\boldsymbol{d} = sym(grad(\boldsymbol{v})) = sym(\dot{\boldsymbol{F}}\boldsymbol{F}^{-1}). \tag{5}$$

These notations and results parallel to those in standard continuum mechanics (e.g., Gurtin et al., 2010).

The swelling ratio, $\Omega \equiv \det(\boldsymbol{F}) > 0$, is the ratio of the volume of a small piece associated with a marker to its volume in the reference configuration. Correspondingly, the instantaneous rate of volume change at a point in the current configuration is the trace of the rate of deformation, $tr(\boldsymbol{d}) = \dot{\Omega}/\Omega$. The rate of shape change is the deviatoric part of the rate of deformation: $\boldsymbol{e} = \boldsymbol{d} - (tr(\boldsymbol{d})/3)\boldsymbol{1}$.

2.2. Balance of forces

The body is subject to a history of mechanical loads, represented by a hanging weight attached to each individual marker (Fig. 2). Let the nominal traction be $\boldsymbol{T}(\boldsymbol{X}, t)$ (i.e., the force on an area in a piece of the solution labeled by the marker $\boldsymbol{X}$ at time t divided by the area of the piece at time 0). Let the body force be $\boldsymbol{B}(\boldsymbol{X}, t)$ (i.e., the force on a piece of the solution labeled by the marker $\boldsymbol{X}$ at time t divided by the volume of the piece at time 0). Let $\boldsymbol{P}$ be the first Piola–Kirchhoff stress tensor (i.e., the force on an area in the current state divided by the area in the reference state). Neglecting inertial effects, the balance of forces requires that

$$\nabla \cdot \boldsymbol{P} + \boldsymbol{B} = \boldsymbol{0}. \tag{6}$$

Balance of moments requires that $\boldsymbol{P}\boldsymbol{F}^T = \boldsymbol{F}\boldsymbol{P}^T$. The nominal traction $\boldsymbol{T}$ acting on an inner surface with outward unit normal $\boldsymbol{N}$ is given by $\boldsymbol{T} = \boldsymbol{P} \cdot \boldsymbol{N}$. On the external surface of the body, mechanical equilibrium requires that

$$\boldsymbol{P} \cdot \boldsymbol{N} = \bar{\boldsymbol{T}}, \tag{7}$$

where $\bar{\boldsymbol{T}}$ is the nominal traction prescribed on the external surface.

2.3. Conservation of molecules

We assume that the two species of molecules A and B do not react to form some other molecules. Consequently, the number of each species of molecules is conserved. Let the nominal concentrations of the two species be $C_A(\boldsymbol{X}, t)$ and $C_B(\boldsymbol{X}, t)$ (i.e., the numbers of molecules in a piece labeled by marker $\boldsymbol{X}$ and at time t divided by the volume of the piece at time 0). The composition of the piece at time t is described by the number fraction of species B:

$$\xi = \frac{C_B}{C_A + C_B}. \tag{8}$$

By definition, ξ is within the range (0, 1). The number fraction of species A is $(1-\xi)$. The function $\xi(\boldsymbol{X}, t)$ describes the field of composition in the body at time t.

Imagine that each piece of the solution is attached to a reservoir of species A and a reservoir of species B (Fig. 2). The piece can absorb or exude molecules in two ways, by exchanging molecules with the reservoirs or by exchanging molecules with neighboring pieces of the solution. Let the rates of species injection from the reservoirs to the body be R_A and R_B (i.e., the numbers of molecules injected from the reservoirs to the piece per unit time divided by the volume of the piece at time 0). Let the nominal diffusion fluxes be $\boldsymbol{J}_A$ and $\boldsymbol{J}_B$ (i.e., the numbers of molecules per unit time crossing an area in the piece per unit area divided by the area in the piece at time 0). The conservation of the two species of molecules requires that:

$$\dot{C}_A = -\nabla \cdot \boldsymbol{J}_A + R_A, \quad \dot{C}_B = -\nabla \cdot \boldsymbol{J}_B + R_B. \tag{9}$$

2.4. Molecular incompressibility

We assume that the binary solution is incompressible, that is, the volume of the solution is independent of the applied stress. The assumption of molecular incompressibility is reasonable provided that the applied stress is small compared to the bulk modulus of the material. Consequently, the volume of the binary solution is a function of the numbers of molecules of A and B only, and the swelling ratio is a function of the nominal concentrations, $\Omega = \Omega(C_A, C_B)$. We define the partial volumes of the two species in the solution as

$$V_A = \frac{\partial \Omega(C_A, C_B)}{\partial C_A}, \quad V_B = \frac{\partial \Omega(C_A, C_B)}{\partial C_B}. \tag{10}$$

Consider a solution of volume V_0 in the reference state. The volume of the solution in the current state is $V_0\Omega$. Since the volume of the solution is an extensive quantity and V_0 is a constant, the function $\Omega(C_A, C_B)$ is homogeneous of degree one and the partial volumes are functions of composition, $V_A(\xi)$ and $V_B(\xi)$. The assumption of molecular incompressibility implies the following relations:

$$\dot{\Omega} = V_A \dot{C}_A + V_B \dot{C}_B. \tag{11}$$

$$\Omega = V_A C_A + V_B C_B. \tag{12}$$

$$0 = \dot{V}_A C_A + \dot{V}_B C_B. \tag{13}$$

Eq. (11) is the definition of the partial volumes V_A and V_B. Eq. (12) results from the properties of homogeneous functions of degree one. Eq. (13) follows from a combination of (11) and (12). For given values of composition ξ and swelling ratio Ω, a combination of (8) and (12) completely specifies the nominal concentrations. In particular, initial nominal concentrations corresponding to a given initial composition field $\xi_0(\boldsymbol{X}) = \xi(\boldsymbol{X}, t = 0)$ can be obtained noting that, by definition, $\Omega = 1$ at time 0.

The assumption of molecular incompressibility does not imply that the partial volumes are constant. By definition, the partial volumes measure the amount by which the solution volume changes by adding an infinitesimal amount of A or B. This amount depends on the physical interactions between the molecules, may be positive or negative, and generally varies with the solution composition. In particular, the partial volumes of the species of molecules in their pure state may differ from their partial volumes in the solution. The volume of the solution then differs from the sum of the volumes that would be occupied by each species of molecules in their pure state. This volume difference is called “volume of mixing” in classical thermodynamics. It vanishes in the particular case where the partial volumes are independent of composition. The notion of volume of mixing is thus distinct from compressibility, which is related to an applied pressure.

The functions $V_A(\xi)$ and $V_B(\xi)$ must be specified as part of the constitutive model, if possible based on experimental observation. Experimental data are commonly summarised by reporting the mean molecular volume of a solution as a function of composition:

$$V_m(\xi) = (1-\xi)V_A(\xi) + \xi V_B(\xi). \tag{14}$$

The mean molecular volume is related to the swelling ratio by: $\Omega = (C_A + C_B)V_m$. The following relations hold (De Voe, 2001):

$$V_A = V_m - \xi \frac{dV_m}{d\xi}, \quad V_B = V_m + (1-\xi)\frac{dV_m}{d\xi}. \tag{15}$$

These relations express the partial volumes in terms of the function $V_m(\xi)$. The relations are the basis for the method of intercepts in classical thermodynamics of solutions. Plot the function $V_m(\xi)$. At a given number fraction ξ, draw the tangent line of the function $V_m(\xi)$. The intersection of the tangent line with the vertical axis at $\xi = 0$ gives $V_A(\xi)$, while the intersection of the tangent line with the vertical axis at $\xi = 1$ gives $V_B(\xi)$.

For later use, we also introduce the volume fraction of species B in the solution as an alternative composition variable:

$$\phi = \frac{V_B C_B}{V_A C_A + V_B C_B}. \tag{16}$$

By definition, the volume fraction is also in the range (0, 1). The volume fraction of species A is $(1-\phi)$. Note that the term "volume fraction" should be used with caution, as the partial volume is not necessarily positive at all compositions (Camacho and Brenner, 1995).

2.5. Free energy

Following the standard practice in continuum irreversible thermodynamics (de Groot and Mazur, 1984), we assume that a free energy function can be defined for each small piece in a non-equilibrium state, and that this function is the same as in the equilibrium state. For simplicity, we limit the theory to isothermal processes, so that the body is held a fixed and constant temperature. We will not list the temperature as a variable. We also neglect the energy of the surface. Let ψ be the nominal Helmholtz free energy density of the solution (i.e., the free energy of a piece at time t divided by the volume of the piece at time 0). Under the assumption of molecular incompressibility, the piece cannot store mechanical energy under an applied pressure by changing volume. It follows that the nominal free energy density is a function of the nominal concentrations only, $\psi = \psi(C_A, C_B)$. We define the partial free energies of the two species in the solution as

$$F_A = \frac{\partial \psi(C_A, C_B)}{\partial C_A}, \quad F_B = \frac{\partial \psi(C_A, C_B)}{\partial C_B}. \tag{17}$$

Since the free energy of a piece of solution associated with a marker is an extensive variable, the function $\psi(C_A, C_B)$ is homogeneous of degree one and the partial free energies are functions of composition, $F_A(\xi)$ and $F_B(\xi)$. The following properties hold:

$$\dot{\psi} = F_A \dot{C}_A + F_B \dot{C}_B. \tag{18}$$

$$\psi = F_A C_A + F_B C_B. \tag{19}$$

$$0 = \dot{F}_A C_A + \dot{F}_B C_B. \tag{20}$$

The functions $F_A(\xi)$ and $F_B(\xi)$ must be specified as part of the constitutive model, if possible based on experimental observation. Experimental data are commonly summarised by reporting the mean molecular free energy of a solution as a function of composition:

$$F_m(\xi) = (1-\xi)F_A(\xi) + \xi F_B(\xi). \tag{21}$$

The mean molecular free energy is related to the nominal free energy density by: $\psi = (C_A + C_B)F_m$. Relations similar to Eq. (15) hold:

$$F_A = F_m - \xi \frac{dF_m}{d\xi}, \quad F_B = F_m + (1-\xi)\frac{dF_m}{d\xi}. \tag{22}$$

These relations express the partial free energies in terms of the function $F_m(\xi)$. The relations are the basis for the method of intercepts in classical thermodynamics of solutions. Plot the function $F_m(\xi)$. At a given number fraction ξ, draw the tangent line of the function $F_m(\xi)$. The intersection of the tangent line with the vertical axis at $\xi = 0$ gives $F_A(\xi)$, while the intersection of the tangent line with the vertical axis at $\xi = 1$ gives $F_B(\xi)$.

2.6. Thermodynamic inequality

The body of solution, the applied forces and the reservoirs together form an isolated system. When the fields of concentration change, the total free energy of the body changes by $\frac{d}{dt}\int \psi dV = \int F_A \dot{C}_A + F_B \dot{C}_B dV$. When the markers move at velocity $\boldsymbol{v}$, the potential energy of the body forces changes at rate $-\int \boldsymbol{B}\cdot\boldsymbol{v}dV$, and the potential energy of the surface forces changes by $-\int \bar{\boldsymbol{T}}\cdot\boldsymbol{v}dS$. The integrals extend over the volume of the body or the surface of body at time 0.

As noted above, each small piece is an open thermodynamic system, connected to reservoirs of A and B. Let the chemical potentials in the reservoirs be $\mu_A(\boldsymbol{X}, t)$ and $\mu_B(\boldsymbol{X}, t)$. The fields of chemical potential in the reservoirs are assumed continuous throughout the body, and equal to the fields of chemical potential in the environment on the surface of the body. In thermodynamic equilibrium, the chemical potential of a species in a piece is defined by its thermodynamic state variables. In a non-equilibrium state, however, we cannot define the chemical potentials in the piece. Rather, we state the thermodynamic inequality as follows.

When molecules migrate from the environment into the body through the surface, the free energy of the environment changes by $\int \mu_A \boldsymbol{J}_A \cdot \boldsymbol{N} + \mu_B \boldsymbol{J}_B \cdot \boldsymbol{N} dS$. When molecules are injected from the reservoirs into the bulk of the body, the free energy of the reservoirs changes by $-\int \mu_A R_A + \mu_B R_B dV$. Thermodynamics requires that the free energy of the isolated system

should never increase:

$$-\int \bar{\boldsymbol{T}}\cdot\boldsymbol{v}dS-\int \boldsymbol{B}\cdot\boldsymbol{v}dV+\int(\mu_A\boldsymbol{J}_A\cdot\boldsymbol{N}+\mu_B\boldsymbol{J}_B\cdot\boldsymbol{N})dS \\ -\int(\mu_A R_A+\mu_B R_B)dV+\int\left(F_A\dot{C}_A+F_B\dot{C}_B\right)dV\le 0. \tag{23}$$

This inequality, along with the compatibility of deformation, balance of forces, and conservation of molecules, implies that

$$\int \boldsymbol{P}:\dot{\boldsymbol{F}}dV+\int\left((\mu_A-F_A)\dot{C}_A+(\mu_B-F_B)\dot{C}_B\right)dV-\int(\boldsymbol{J}_A\cdot\nabla\mu_A+\boldsymbol{J}_B\cdot\nabla\mu_B)dV\ge 0. \tag{24}$$

In deriving the above equation, we have also used the divergence theorem. Since the inequality must hold for any subpart of the body, it implies that

$$\boldsymbol{P}:\dot{\boldsymbol{F}}+(\mu_A-F_A)\dot{C}_A+(\mu_B-F_B)\dot{C}_B-\boldsymbol{J}_A\cdot\nabla\mu_A-\boldsymbol{J}_B\cdot\nabla\mu_B\ge 0. \tag{25}$$

Note the identity $\boldsymbol{P}:\dot{\boldsymbol{F}}=\sigma_m\dot{\Omega}+\Omega\boldsymbol{s}:\boldsymbol{e}$, with σ_m being the mean Cauchy stress and $\boldsymbol{s}=\boldsymbol{\sigma}-\sigma_m\boldsymbol{1}$ being the deviatoric Cauchy stress. Using the incompressibility condition (11), we rewrite the inequality (25) as

$$\left(\frac{\mu_A-F_A}{V_A}+\sigma_m\right)V_A\dot{C}_A+\left(\frac{\mu_B-F_B}{V_B}+\sigma_m\right)V_B\dot{C}_B+\Omega\boldsymbol{s}:\boldsymbol{e}-\boldsymbol{J}_A\cdot\nabla\mu_A-\boldsymbol{J}_B\cdot\nabla\mu_B\ge 0. \tag{26}$$

The left-hand side of the inequality represents the rate of dissipation of a piece at time t divided by the volume at time 0. The equality holds when the composite isolated system is in a state of thermodynamic equilibrium, and the inequality holds when the composite isolated system is not in a state of equilibrium.

The inequality is rewritten in terms of true quantities in the following way. Define the true rates of volumetric insertion $i_A=V_A\dot{C}_A/\Omega$ and $i_B=V_B\dot{C}_B/\Omega$ (Brassart et al., 2016). Note that $tr(\boldsymbol{d})=i_A+i_B$. Introduce the true diffusion fluxes (number of molecules crossing per unit reference area), which are related to the nominal diffusion fluxes by: $\boldsymbol{j}_A=\Omega^{-1}\boldsymbol{F}\cdot\boldsymbol{J}_A$, $\boldsymbol{j}_B=\Omega^{-1}\boldsymbol{F}\cdot\boldsymbol{J}_B$ (Hong et al., 2008). The inequality (26) becomes

$$\left(\frac{\mu_A-F_A}{V_A}+\sigma_m\right)i_A+\left(\frac{\mu_B-F_B}{V_B}+\sigma_m\right)i_B+\boldsymbol{s}:\boldsymbol{e}-\boldsymbol{j}_A\cdot grad(\mu_A)-\boldsymbol{j}_B\cdot grad(\mu_B)\ge 0. \tag{27}$$

The inequality (27) involves thirteen independent rates (i_A, i_B, $\boldsymbol{e}$, $\boldsymbol{j}_A$, $\boldsymbol{j}_B$) and identifies their conjugate thermodynamic forces (ζ_A, ζ_B, $\boldsymbol{s}$, $grad(\mu_A)$, $grad(\mu_B)$). The thermodynamic forces conjugate to the rate of volumetric insertion ζ_A and ζ_B were introduced in Brassart et al. (2016) and are defined as $\zeta_A\equiv(\mu_A-F_A)/V_A+\sigma_m$ and $\zeta_B\equiv(\mu_B-F_B)/V_B+\sigma_m$. They have the dimension of stress and involve a combination of mechanical and chemical forces. The thermodynamic driving force conjugate to the deviatoric rate of deformation $\boldsymbol{e}$ is identified as the deviatoric Cauchy stress $\boldsymbol{s}$.[1] Finally, the driving force for long-range migration of species is identified as the gradient of chemical potential, $grad(\mu_A)$ and $grad(\mu_B)$. In the following, we satisfy the inequality (27) by prescribing kinetic models that relate the rates to their conjugate forces.

Note that here we did not a priori postulate a dependence of chemical potential on concentration. In fact, in our presentation so far chemical potentials are treated as prescribed chemical body forces that are independent of concentration. Consequently, the traditional Coleman and Noll argument (see e.g. Gurtin et al., 2010) that would lead to the assumption of local chemical equilibrium does not hold.

3. Constitutive theory

3.1. Free energy function

We specify the partial free energy function $F_A(\xi)$ and $F_B(\xi)$ by adopting the model for ideal mixing of molecules of unequal size proposed in Brassart et al. (2016). In contrast with classical thermodynamic models of solutions (e.g. Flory, 1942), this model does not rely on a lattice model, and can therefore handle nonzero volume of mixing. The model is based on the very strong assumption that molecules do not interact with each other and are therefore free to explore the entire configuration space. Starting from this postulate, the difference in the number of configurations of molecules between the unmixed and mixed states, i.e. the entropy of mixing ΔS^{mix}, is readily calculated. The corresponding change in free energy is then given by $\Delta F^{mix}=-kT\Delta S^{mix}$ (for ideal mixing, we also assume that the energy of mixing vanishes). The partial free energies of the model of ideal mixing are given by (see Brassart et al. (2016)):

$$F_A(\xi)=F_A^o+kT\left[\log\frac{(1-\xi)V_A(0)}{V_m(\xi)}+\frac{\xi\left(V_B(\xi)-V_A(\xi)\right)}{V_m(\xi)}\right] \tag{28}$$

[1] In textbooks on irreversible thermodynamics, the stress is referred to as the thermodynamic flux (flux of momentum) and the velocity gradient as its conjugate force. Here we view the deviatoric stress as the cause for flow, and therefore call deviatoric stress the force and deviatoric strain rate the conjugated flux. Consistently, the mean stress contributes to the force for species insertion.

$$F_B(\xi) = F_B^o + kT\left[\log\frac{\xi V_B(1)}{V_m(\xi)} + \frac{(1-\xi)(V_A(\xi)-V_B(\xi))}{V_m(\xi)}\right] \tag{29}$$

where F_A^o and F_B^o are the partial free energies of molecules A and B in their pure state, and $V_m(\xi)$ is the mean molecular volume, defined in Eq. (14). Remarkably, this simple model recovers the Flory–Huggins model (assuming no energy of mixing) when the volume of mixing is absent (i.e. when the partial volumes do not vary with composition). It further reduces to the ideal solution model when the partial volumes of the two species are identical.

3.2. Kinetic model of species insertion and flow

We satisfy the thermodynamic inequality (27) by prescribing kinetic models for local (flow and species insertion) and long-range (diffusion) processes separately. The simplest kinetic model for species insertion coupled to flow assumes that the solution is isotropic, and that the relationship between the thermodynamic forces and the fluxes is linear. Another requirement is that the kinetic model should be independent of the choice of a reference configuration (we assume that the solution has no memory of its initial state).

We adopt the linear model previously proposed in Brassart et al. (2016):

$$\boldsymbol{s} = 2\eta\boldsymbol{e} \tag{30}$$

$$\frac{\mu_A - F_A}{V_A} + \sigma_m = \beta_{AA} i_A + \beta_{AB} i_B \tag{31}$$

$$\frac{\mu_B - F_B}{V_B} + \sigma_m = \beta_{BA} i_A + \beta_{BB} i_B \tag{32}$$

Eq. (30) is the classical model of Newtonian flow with $\eta = \eta(\xi)$ and describes the kinetics of shape change of the solution. Eqs. (31) and (32) describe the kinetics of volume change due to the insertion of species. The viscosity-like coefficients $\beta_{\alpha\beta}(\xi)$ (α, β=A,B) represent the resistance to the insertion of species within an element of volume as defined by markers. At the molecular scale, this resistance is attributed to the breaking and reforming of bonds. We assume the Onsager reciprocity: $\beta_{AB} = \beta_{BA}$ and also that $\beta_{AA} > 0$, $\beta_{BB} > 0$ and $\beta_{AA}\beta_{BB} - \beta_{AB}^2 > 0$ to ensure that the dissipation is always non-negative. The conditions of equilibrium, steady states and homogeneous states were discussed in Brassart et al. (2016).

The right-hand sides of (31) and (32) are easily expressed in terms of nominal concentrations recalling that $i_A = V_A\dot{C}_A/\Omega$ and $i_B = V_B\dot{C}_B/\Omega$:

$$\frac{\mu_A - F_A}{V_A} + \sigma_m = \frac{\beta_{AA}}{\Omega} V_A\dot{C}_A + \frac{\beta_{AB}}{\Omega} V_B\dot{C}_B \tag{33}$$

$$\frac{\mu_B - F_B}{V_B} + \sigma_m = \frac{\beta_{BA}}{\Omega} V_A\dot{C}_A + \frac{\beta_{BB}}{\Omega} V_B\dot{C}_B \tag{34}$$

The kinetic model (33) and (34) provides evolution equations for the nominal concentrations as a function of the applied chemical and mechanical load in a material element associated with a marker.

In the following we will assume that the cross coefficient β_{AB} vanishes for simplicity, and write $\beta_A \equiv \beta_{AA}$ and $\beta_B \equiv \beta_{BB}$ for conciseness.

3.3. Kinetic model of long-range transport of species

We assume that long-range transport of molecules is governed by diffusion and write the kinetic model under the form:

$$\boldsymbol{j}_A = -c_A M_A \mathrm{grad}(\mu_A), \quad \boldsymbol{j}_B = -c_B M_B \mathrm{grad}(\mu_B) \tag{35}$$

where $\boldsymbol{j}_\alpha$ is the number of α molecules per unit time and area in the current configuration, c_α the number of molecules per unit volume in the current configuration, and M_α is the mobility of species α. By definition, the mobility M_α is the proportionality ratio between the diffusion "velocity", $\boldsymbol{j}_\alpha/c_\alpha$, and the driving force $\mathrm{grad}(\mu_\alpha)$. For simplicity, we neglect the effect that the gradient of the chemical potential of one species drives the flux of the other species. Eq. (35) represent an updated Lagrangian description of diffusion, with the quantities $\boldsymbol{j}_\alpha$, c_α and μ_α associated with the markers. In particular, the diffusion velocity $\boldsymbol{j}_\alpha/c_\alpha$ represents the velocity of molecules α relative to the bulk motion as defined by the marker velocity. This view is consistent with Darken's description of diffusion fluxes (Darken, 1948), see also Sekerka (2004).

The kinetic model (35) can be recast in terms of nominal quantities. The true and nominal concentrations are related by $c_\alpha = C_\alpha/\Omega$, and recall that $\boldsymbol{j}_\alpha = \Omega^{-1}\boldsymbol{F}\cdot\boldsymbol{J}_\alpha$. The kinetic model (35) becomes:

$$\boldsymbol{J}_A = -C_A M_A(\boldsymbol{F}^{-1}\boldsymbol{F}^{-T})\cdot\nabla\mu_A, \quad \boldsymbol{J}_B = -C_B M_B(\boldsymbol{F}^{-1}\boldsymbol{F}^{-T})\cdot\nabla\mu_B. \tag{36}$$

These relations show that the proportionality coefficients in the Lagrangian description are anisotropic and depend on the deformation gradient, as well as on composition.

4. Summary of the theory of poroviscosity and boundary value problems

Sections 2 and 3 form a complete theory of poroviscosity. Given continuous fields of chemical potential μ_A and μ_B and body force $\boldsymbol{B}$, Eqs. (4) and (5) (kinematics), (6) (force balance), (9) (conservation of species), (12) (incompressibility), (30) (flow), (33) and (34) (insertion), and (36) (diffusion) provide 34 relations to evolve 34 fields: $\boldsymbol{\chi}$, $\boldsymbol{F}$, $\boldsymbol{d}$, $\boldsymbol{\sigma}$, R_A, R_B, C_A, C_B, $\boldsymbol{J}_A$, $\boldsymbol{J}_B$. The composition is calculated from the nominal concentrations using Eq. (8). Boundary conditions are written in terms of prescribed tractions and prescribed chemical potentials on the external surface.

4.1. Vanishing source term

Our theory so far assumes prescribed fields of chemical potentials and treats the source terms R_A and R_B in the species conservation Eq. (9) as the unknowns. In practical problems however, often there are no reservoirs connected to material elements within the body, and the source term in the species conservation equations should vanish in (9): $R_A = 0$ and $R_B = 0$:

$$\dot{C}_A = -\nabla \cdot \boldsymbol{J}_A, \quad \dot{C}_B = -\nabla \cdot \boldsymbol{J}_B. \tag{37}$$

Fields of chemical potential μ_A and μ_B should then be calculated such that Eq. (37) are satisfied. They should also satisfy boundary conditions in terms of prescribed chemical potentials on the external surface, corresponding to prescribed chemical potentials in the environment. This approach amounts to considering chemical potentials as Lagrange multipliers enforcing species conservation, similarly to the treatment of Larché and Cahn (1985). Actually, we could have developed our theory by enforcing (37) in the dissipation inequality through Lagrange multipliers, and without including reservoirs.

The presentation based on fields of reservoirs provides a physical interpretation of chemical potential even when local chemical equilibrium is not met in the body. By adjusting the well-defined chemical potentials in the reservoirs in such a way that the injection rates vanish, we establish chemical equilibrium between the reservoir and a small piece in the body. Reservoirs can thus be viewed as devices that measure chemical potential within a body. This is similar to a thermometer measuring temperature: at thermal equilibrium, the temperatures in the piece and in the thermometer are identical.

4.2. Boundary value problems

In the rest of the paper, we will only consider the situation where the injection rates from the reservoir to the body vanish, and Eq. (37) hold. We view the fields of chemical potential $\mu_A(\boldsymbol{X}, t)$ and $\mu_B(\boldsymbol{X}, t)$ as our primary unknowns, alongside the displacement field $\boldsymbol{u}(\boldsymbol{X}, t) = \boldsymbol{\chi}(\boldsymbol{X}, t) - \boldsymbol{X}$. These five fields must satisfy five coupled, nonlinear Partial Differential Equations (PDEs):

$$\boldsymbol{0} = \nabla \cdot \boldsymbol{P} + \boldsymbol{B} \tag{38}$$

$$\dot{C}_A = -\nabla \cdot \boldsymbol{J}_A \tag{39}$$

$$\dot{C}_B = -\nabla \cdot \boldsymbol{J}_B \tag{40}$$

In Eq. (38), the first Piola-Kirchhoff stress is related to the Cauchy stress by $\boldsymbol{P} = (\det(\boldsymbol{F}))\boldsymbol{\sigma}\boldsymbol{F}^{-T}$. The deviatoric Cauchy stress is in turn related to the deviatoric part of the rate of deformation by the kinetic model of flow (30). In (39) and (40), the rates of change of nominal concentrations $\dot{C}_A$ and $\dot{C}_B$ are related to the chemical potentials by the kinetic model of insertion (33) and (34), and the nominal diffusion fluxes $\boldsymbol{J}_A$ and $\boldsymbol{J}_B$ are related to the gradients of chemical potential by the kinetic model of diffusion (36). Eqs. (39) and (40) are thus PDEs for the fields of chemical potential, whereas the nominal concentrations are treated as internal variables. The mean Cauchy stress σ_m is not prescribed constitutively, and should be determined such that the local incompressibility condition (12) is satisfied. For given values of composition ξ, swelling ratio $\Omega = \det(\boldsymbol{F})$ and chemical potentials at a point, the rates of nominal concentrations and mean Cauchy stress can be calculated by solving simultaneously the algebraic system of Eqs. (33), (34) and (12).

The boundary conditions for the mechanical problem are written in terms of imposed displacement on a part S_u of the external surface, and imposed tractions on the complementary part S_T, so that $S_u \cup S_T = S$ and $S_u \cap S_T = \emptyset$:

$$\boldsymbol{u}(\boldsymbol{X}, t) = \bar{\boldsymbol{u}}(\boldsymbol{X}, t) \text{ for } \boldsymbol{X} \text{ on } S_u, \tag{41}$$

$$\boldsymbol{P}(\boldsymbol{X}, t) \cdot \boldsymbol{N}(\boldsymbol{X}, t) = \bar{\boldsymbol{T}}(\boldsymbol{X}, t) \text{ for } \boldsymbol{X} \text{ on } S_T. \tag{42}$$

The boundary conditions for the chemical problem consist in prescribed chemical potential on a portion S_{μ_α} of the boundary, and prescribed net flux on the complementary portion S_{J_α}, so that $S_{\mu_\alpha} \cup S_{J_\alpha} = S$ and $S_{\mu_\alpha} \cap S_{J_\alpha} = \emptyset$, where the net flux through a surface is defined as $J_\alpha = -\boldsymbol{J}_\alpha \cdot \boldsymbol{N}$:

$$\mu_\alpha(\boldsymbol{X}, t) = \bar{\mu}_\alpha(\boldsymbol{X}, t) \text{ for } \boldsymbol{X} \text{ on } S_{\mu_\alpha}, \tag{43}$$

$$-\boldsymbol{J}_\alpha(\boldsymbol{X}, t) \cdot \boldsymbol{N}(\boldsymbol{X}, t) = \bar{J}_\alpha(\boldsymbol{X}, t) \text{ for } \boldsymbol{X} \text{ on } S_{J_\alpha}. \tag{44}$$

5. Weak formulation and finite element solution procedure

In this section we turn to the numerical implementation of the theory of poroviscosity with the finite element method. As is standard, the weak form of the mechanical problem is obtained by multiplying the balance Eq. (6) by a vector test function $\hat{\boldsymbol{u}}$ that vanishes on S_u, integrating over the reference volume of the body, using the divergence theorem and the boundary conditions (41) and (42) to finally obtain:

$$\int \boldsymbol{P} : \nabla \hat{\boldsymbol{u}} dV = \int \hat{\boldsymbol{u}} \cdot \boldsymbol{B} dV + \int_{S_T} \hat{\boldsymbol{u}} \cdot \bar{\boldsymbol{T}} dS. \tag{45}$$

Similarly, the weak form of the chemical problem is obtained by multiplying the species conservation Eq. (37) by scalar test functions $\hat{\mu}_A$ and $\hat{\mu}_B$ that vanish on S_{μ_A} and S_{μ_B}, respectively. Integration over the reference volume of the body and use of the divergence theorem and the boundary conditions (43) and (44) lead to:

$$\int \left(\dot{C}_A \hat{\mu}_A - \boldsymbol{J}_A \cdot \nabla \hat{\mu}_A\right) dV = \int_{S_{J_A}} \hat{\mu}_A \bar{J}_A dS, \tag{46}$$

$$\int \left(\dot{C}_B \hat{\mu}_B - \boldsymbol{J}_B \cdot \nabla \hat{\mu}_B\right) dV = \int_{S_{J_B}} \hat{\mu}_B \bar{J}_B dS. \tag{47}$$

The weak forms (45)–(47) are discretized in space using finite element interpolations of the unknown fields $\boldsymbol{u}$, μ_A and μ_B:

$$\boldsymbol{u} = \sum \boldsymbol{u}^I N^I, \quad \mu_A = \sum \mu_A^I N^I, \quad \mu_B = \sum \mu_B^I N^I. \tag{48}$$

In (48), the index $I = 1, \ldots, N$ is the node number, $\boldsymbol{u}^I$, μ_A^I and μ_B^I are the nodal displacements and chemical potentials, and N^I the shape functions. We adopt a standard Galerkin formulation and use the same shape functions to interpolate the test functions $\hat{\boldsymbol{u}}$, $\hat{\mu}_A$ and $\hat{\mu}_B$. We obtain the following $(5 \times N)$ equations for $(5 \times N)$ nodal values:

$$\int \boldsymbol{P} : \nabla N^I dV = \int \boldsymbol{B} N^I dV + \int_{S_T} \bar{\boldsymbol{T}} N^I dS \tag{49}$$

$$\int \left(\dot{C}_A N^I - \boldsymbol{J}_A \cdot \nabla N^I\right) dV = \int_{S_{J_A}} \bar{J}_A N^I dS \tag{50}$$

$$\int \left(\dot{C}_B N^I - \boldsymbol{J}_B \cdot \nabla N^I\right) dV = \int_{S_{J_B}} \bar{J}_B N^I dS \tag{51}$$

As is standard, the integrals are evaluated numerically using an appropriate quadrature method. At every integration point, the nominal stress, concentration rates and diffusion fluxes are related to the displacement and chemical potential through the kinematic relations, incompressibility condition and kinetic models. In particular, as mentioned in Section 4.2, incompressibility is handled at the level of each integration point by numerically solving Eqs. (12), (33) and (34) simultaneously for the nominal concentrations and mean stress. The deviatoric stress can then be calculated explicitly from (30), and the diffusion fluxes from (36). Integration in time is done using a fully implicit, backward Euler scheme, leading to a system of $(5 \times N)$ nonlinear equations, which is solved at every time step using a Newton–Raphson scheme.

The advantage of using chemical potential as a nodal variable (instead of concentration) is that the evaluation of the gradient of chemical potential at integration points needed to calculate the diffusion flux is straightforward. Using the concentration would have required the calculation of the gradient of mean stress. A (comparatively minor) drawback is that it requires the numerical inversion of the partial free energy functions (28) and (29). The advantage of using chemical potential as primary field was recognized in other works (e.g. Chester et al., 2015).

6. Numerical examples

6.1. Interdiffusion in an 1D unbounded, periodic system

We consider a periodic system consisting of alternating layers of A-rich and B-rich solutions (Fig. 3). The in-plane dimensions of the layers are assumed much larger than the out-of-plane dimension, so that diffusion takes place only in the out-of-plane, x-direction. We write the stretch in the x-direction: $\lambda_x = \partial x / \partial X$, and the swelling ratio is given by $\Omega = \lambda_x$. The system is subject to no applied traction in the x-direction, so that mechanical equilibrium reduces to $\sigma_{xx} = 0$. We assume that the system is constrained in the y- and z-directions, so that $d_{yy} = d_{zz} = 0$. This kinematic constraint introduces a state of biaxial stress $\sigma_{yy} = \sigma_{zz}$ that couples the change of volume and the change of shape. Due to periodicity, we only consider a 1D unit cell occupying the region $-L < X < L$ in the reference configuration. In the initial state, the composition of the A-rich $(-L < X < 0)$ and B-rich $0 < X < L$ solution layers are written ϕ_0^1 and ϕ_0^2 respectively. We choose the initial state as the reference state. At times $t > 0$, the system homogenizes by interdiffusion.

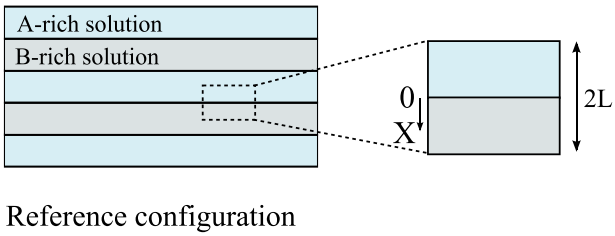

Fig. 3. At time 0, a binary solution has alternating A-rich and B-rich layers of two uniform compositions (left). The system is initially stress-free. The solution homogenizes by flow and diffusion. A periodic unit cell is used for numerical analysis (right).

We numerically solve the species conservation Eq. (37) for the two unknown fields $\mu_A(X,\, t)$ and $\mu_B(X,\, t)$, implicitly accounting for mechanical equilibrium and the kinematic constraints. Natural boundary conditions are used to satisfy periodicity: $J_A(\pm L, t) = J_B(\pm L, t) = 0$. In 1D, the finite element discretizations (50) and (51) reduce to

$$\int_{-L}^{L} \left(\dot{C}_A N^I - J_A \frac{\partial N^I}{\partial X} \right) dX = 0, \tag{52}$$

$$\int_{-L}^{L} \left(\dot{C}_B N^I - J_B \frac{\partial N^I}{\partial X} \right) dX = 0. \tag{53}$$

At every integration point, the constitutive Eqs. (33)-(34) for the insertion of species A and B are solved simultaneously to update the nominal concentrations:

$$\frac{\mu_A - F_A}{V_A} - \frac{4}{3}\eta \frac{\dot{\lambda}_x}{\lambda_x} = \beta_A V_A \frac{\dot{C}_A}{\Omega} \tag{54}$$

$$\frac{\mu_B - F_B}{V_B} - \frac{4}{3}\eta \frac{\dot{\lambda}_x}{\lambda_x} = \beta_B V_B \frac{\dot{C}_B}{\Omega} \tag{55}$$

In writing (54) and (55), we have used the model of shear viscosity (30) to relate the mean stress to the change of volume, taking into account the kinematic constraint on the deformations: $\sigma_m = -4\eta\dot{\lambda}_x/3\lambda_x$. We have also neglected the cross terms in the kinetic model of species insertion. The stretching rate $\dot{\lambda}_x = \dot{\Omega}$ is directly related to the change in nominal concentrations through the incompressibility constraint (11). The diffusion fluxes in (52) and (53) are given by

$$J_A = -\frac{C_A M_A}{\lambda_x^2} \frac{\partial \mu_A}{\partial X}, \; J_B = -\frac{C_B M_B}{\lambda_x^2} \frac{\partial \mu_B}{\partial X}. \tag{56}$$

We emphasize that no specific treatment of the discontinuity in the initial composition field is required within our numerical scheme, since the concentrations are treated as internal variables and are updated at the level of the integration point. On the other hand, the fields of chemical potential are continuous. Eqs. (52) and (53) are discretized in time using the fully implicit backward Euler scheme. The weak form is discretized in space with 100 elements, and linear shape functions were used. Convergence of the results in both space and time was verified numerically. In the simulations, we used $\phi_0^1 = 0.25$ and $\phi_0^2 = 0.75$. The material parameters are the following: $M_B/M_A = 100$, $V_B/V_A = 0.1$ and $\beta_A/\eta = \beta_B/\eta = 1$. We neglect the volume of mixing and assume constant partial volumes.

Fig. 4 shows the profiles of composition, chemical potential and mean stress for varying size of the unit cell L relative to the poroviscous length $\Lambda = \sqrt{M_B V_B \eta}$. Time is normalized by the characteristic time for diffusion of the fast species, $\tau_D = L^2/D_B$ with $D_B = M_B kT$ the diffusion coefficient of species B. When $L/\Lambda = 10$ (Fig. 4(a) and (b)), viscous relaxation is faster than diffusion. Associated with local deformation, an internal stress builds up (Fig 4(c)), but its contribution to the driving force for diffusion is negligible in comparison to the chemical contribution. Since bulk viscous relaxation is complete at these time scales, local chemical equilibrium is satisfied. Continuity in chemical potential (Fig. 4(b)) then leads to continuity in composition throughout the unit cell.

When $L/\Lambda = 1$, bulk viscous relaxation is not completed at the considered times (Fig. 4(d)–(f)). Consequently, local chemical equilibrium is not reached, and the concentration is discontinuous at the interface (Fig. 4(d)), although the chemical potential is continuous throughout the cell (Fig. 4(e)). The mean stress is also discontinuous, and is one order of magnitude larger than in Fig. 4(c) as it has not yet relaxed by viscous flow. The corresponding stress gradient slows down the diffusion of species B, but accelerates that of species A. The overall effect of stress on diffusion leads to a more homogeneous profile of chemical potential (Fig. 4(e)), as compared to the almost stress-free situation (Fig. 4(b)).

For even smaller system size, $L/\Lambda = 0.1$ (Fig. 4(g)–(i)), diffusion is much faster than viscous relaxation, and the composition profile is practically piecewise uniform (Fig. 4(g)), with a discontinuity at the interface. Profiles of chemical potential are also flat and continuous throughout the cell. Due to the small concentration gradients, the stress is also very low (Fig. 4(i)).

While the finite element numerical solution is robust and able to handle strong nonlinearities, as well as jumps in the concentration fields, it is still enlightening to consider the analytical solution to a closely related interdiffusion problem. We

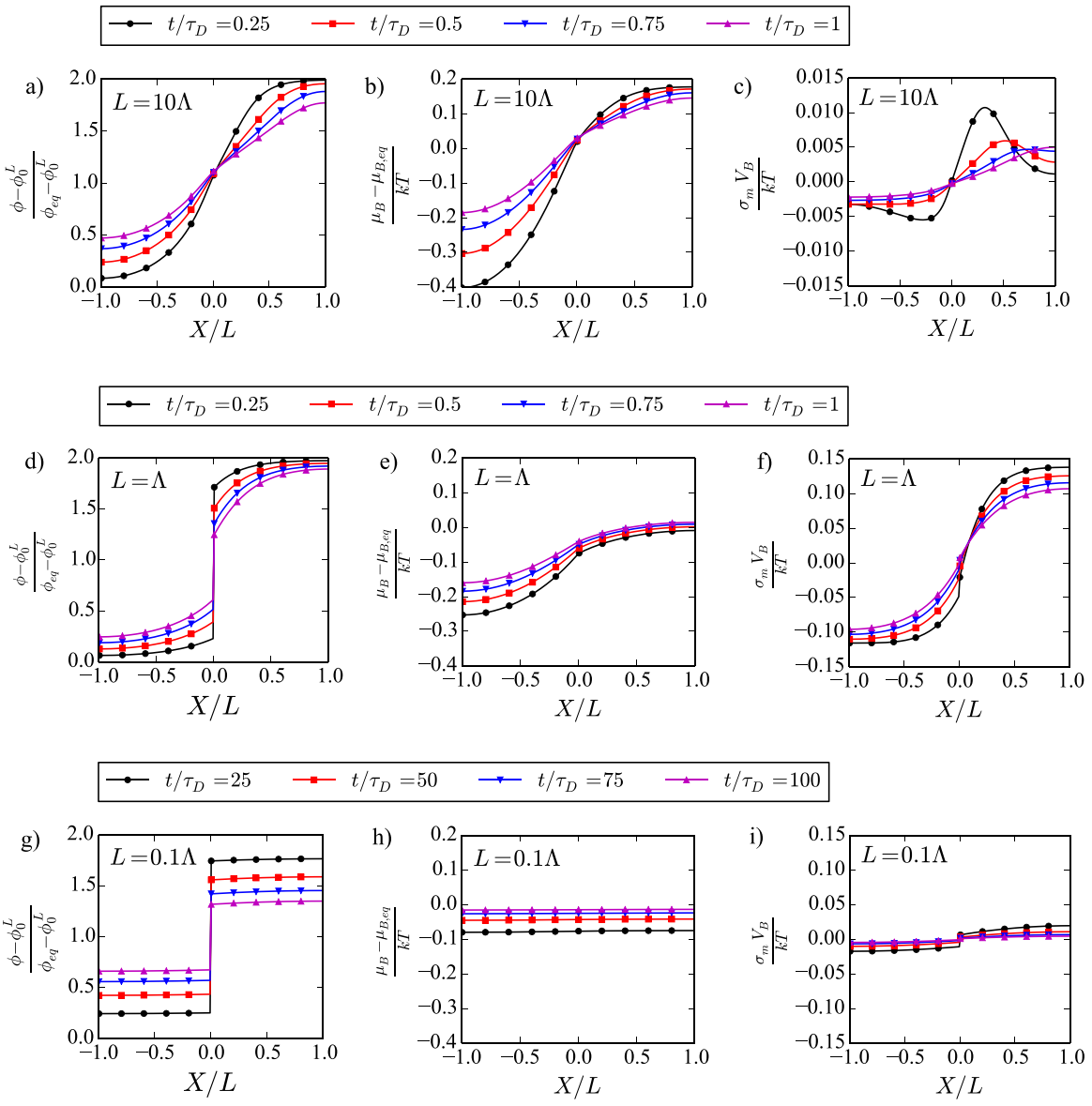

Fig. 4. Profiles of volume fraction ϕ, chemical potential μ_B and mean stress σ_m, in bilayer systems of varying length: (a,b,c): $L = 10\Lambda$, (d,e,f): $L = \Lambda$, (g,h,i): $L = 0.1\Lambda$, at various times. In the legend, time is normalized by the characteristic time for diffusion of species B, $\tau_D = L^2/D_B$ with $D_B = M_B kT$. As the system size is reduced, mixing is limited by local insertion of species, rather than by diffusion.

now consider small perturbations of the composition field about the uniform equilibrium value in a binary solution, and seek to determine the overall relaxation time of the system in analytical form. This problem was previously considered by Stephenson (1988). Here we have generalized Stephenson's derivations to also account for the kinetics of species insertion. Details about the methodology can be found in Appendix B, as well as in Stephenson's paper.

The perturbation analysis provides the relaxation time of a harmonic compositional fluctuation with wavelength λ, as shown in Fig. 5, for different values of the viscosity parameters. Material parameters and the equilibrium composition are the same as in Fig. 4.

- For composition fluctuations of large wavelength, the relaxation of the system is limited by diffusion, with relaxation time scaling with the square of the diffusion characteristic length, λ^2. Stress is negligible and Darken's original analysis is recovered. This situation was illustrated with the numerical solutions in Fig. 4(a)–(c).
- In the small wavelength limit, the relaxation of the system is limited by the kinetics of species insertion, and the relaxation time does not depend on the wavelength (but does depend on the bulk viscosity). This situation was illustrated with the numerical solutions in Fig. 4(g)–(i).

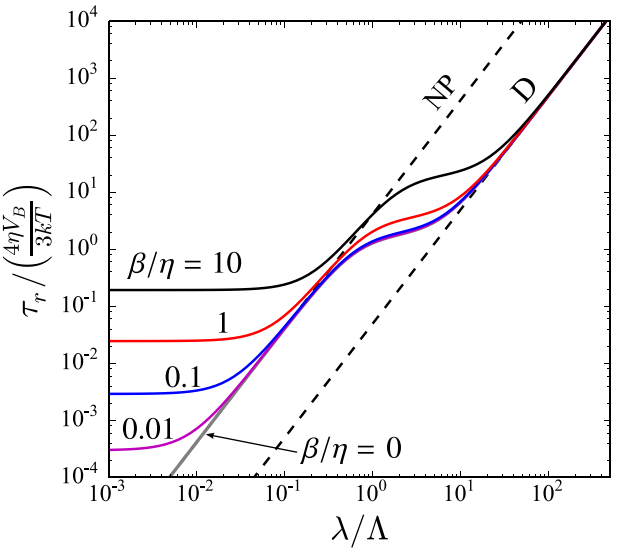

Fig. 5. Interdiffusion relaxation time τ_r as function of the wavelength λ of a composition perturbation in a 1D system initially at equilibrium, for varying values of the bulk viscosity-to-shear viscosity ratio. The relaxation time is normalized by a characteristic viscous time $\tau_v = 4\eta V_B/3kT$, and the wavelength is normalized by the poroviscous length Λ. For perturbations of small wavelengths, relaxation is limited by local species insertion into the bulk, and is size-independent. When local chemical equilibrium is assumed ($\beta = 0$), the relaxation time tends to the Nernst-Planck (NP) asymptote. For sufficiently large perturbation wavelengths, the relaxation is limited by diffusion, and the relaxation time tends to the Darken (D) asymptote, at all values of the viscosity coefficients.

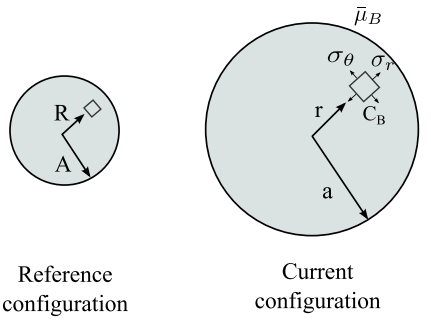

Fig. 6. The boundary-value problem of a body of a binary solution in which only one species (B) can diffuse. The solution is immersed in a bath of another solution in which the chemical potential of molecules of B, $\bar{\mu}_B$, is fixed. The reference configuration is defined as the "dry" state in which the concentration in molecules of B is zero. In the current state, the body swells by absorbing molecules of B.

- When the bulk viscosity is set to zero, keeping the shear viscosity finite, another diffusion-limited regime is reached in the small wavelength limit. This regime was previously identified by Stephenson and is referred to as the Nernst-Planck regime.[2] In this regime viscous flow is negligible, and mixing proceeds by swapping the volumes of the interdiffusing species to satisfy incompressibility. This results from the large stress gradient that tends to accelerate the diffusion of the slow species and to slow down the diffusion of the fast species. Note that Stephenson considered only the case $\beta = 0$. When $\beta \neq 0$, the range of wavelengths at which the Nernst-Planck regime prevails is very limited.

A more detailed account of the implications of these three regimes in relation with effective interdiffusion coefficients is given in Appendix B.

6.2. Free swelling of a particle

We now consider the swelling of a spherical particle of a binary solution of species A and B (Fig. 6). We assume that the mobility of the molecules of B is much larger than that of the molecules of A, $M_B \gg M_A$, and neglect the diffusion of molecules of A. We use the dry state ($C_B = 0$) as the reference configuration. Since the diffusion of A is neglected, species

[2] This regime was called "Nernst-Planck" by Stephenson in reference to the Nernst-Planck analysis of interdiffusion of charged species where an electrostatic potential couples the diffusion fluxes to maintain electroneutrality (Doremus, 1964).

A becomes the markers. The nominal concentration C_A in the particle is uniform at all times and equals the nominal concentration in the dry state, such that $V_A C_A = 1$. Let A be the outer radius of the particle in the reference state, and write R the radial position of a material element in the reference configuration (Fig. 6(a)). At time $t = 0$ and afterwards, the particle is immersed in a bath of another solution in which the chemical potential of B is $\bar{\mu}_B$. We assume that the external surface of the particle is stress free, and neglect body forces. The particle then swells by absorbing molecules of B from the bath. A similar boundary-value problem has been used to model concurrent diffusion and plastic flow in lithium-ion batteries (Brassart et al., 2013; Zhao et al., 2011), where local chemical equilibrium was assumed.

Accounting for the spherical symmetry of the problem and using spherical coordinates, the boundary value problem is rewritten as a 1D problem. The unknown fields are the current position of markers, $r(R, t)$, and the chemical potential of species B, $\mu_B(R, t)$. The radial and hoop stretches are $\lambda_r = \partial r/\partial R$ and $\lambda_\theta = r/R$, and the swelling ratio is $\Omega = \lambda_r \lambda_\theta^2$. As the nominal concentration of A is constant, it follows that the nominal concentration of B is one-to-one related to the stretches by the incompressibility condition (12):

$$\lambda_r \lambda_\theta^2 = 1 + V_B C_B. \tag{57}$$

The mean stress can then be calculated explicitly from the kinetic model (34). The radial and hoop stretching rates are given by $d_r = \dot{\lambda}_r/\lambda_r$ and $d_\theta = \dot{\lambda}_\theta/\lambda_\theta$, and the shear stresses are calculated as:

$$s_r = \frac{4\eta}{3}(d_r - d_\theta), \quad s_\theta = \frac{2\eta}{3}(d_\theta - d_r). \tag{58}$$

The radial and hoop components of the first Piola–Kirchhoff stress are related to the components of the Cauchy stress by $P_r = \lambda_\theta^2(s_r + \sigma_m)$ and $P_\theta = \lambda_r \lambda_\theta (s_\theta + \sigma_m)$. Finally, the radial diffusion flux of molecules of B is given by:

$$J_B = -\frac{C_B M_B}{\lambda_r^2}\frac{\partial \mu_B}{\partial R}. \tag{59}$$

The finite element discretizations (49) and (51) become

$$\int_0^A \left(P_r \frac{\partial N^I}{\partial R} + 2P_\theta \frac{N^I}{R}\right) R^2 dR = 0, \tag{60}$$

$$\int_0^A \left(\dot{C}_B N^I - J_B \frac{\partial N^I}{\partial R}\right) R^2 dR = 0. \tag{61}$$

The finite element system (60) and (61) is integrated in time using the fully implicit backward Euler scheme. We use 100 elements with linear shape functions, with one integration point per element.

Define a characteristic time for viscous relaxation, $\tau_\nu = \eta V_B/kT$ and a characteristic time for diffusion, $\tau_D = A^2/D_B$, with $D_B = M_B kT$ the diffusion coefficient of species B. The viscous relaxation time and the mobility together define a poroviscous length, $\Lambda = \sqrt{M_B V_B \eta}$, which represents the distance of the migration of species B within a time comparable to the time for viscous relaxation. The swelling of the particle is then completely described by the following dimensionless parameters: A/Λ, β/η, and V_B/V_A, with $\beta \equiv \beta_B$. In the following, we will investigate the effect of the first two parameters, taking $V_B/V_A = 0.1$. The initial volume fraction of B is set to $\phi(R, 0) = 0.25$, which corresponds to an initial particle radius $a(0) = 1.1A$. The chemical potential of B in the bath is set to $\bar{\mu}_B = F_B(\phi_{eq})$, with $\phi_{eq} = 0.5$.

Profiles of composition, chemical potential and mean stress for $\beta/\eta = 1$ and three particle radii are shown in Fig. 7. When the particle size is large compared to the poroviscous length ($A/\Lambda = 10$, Fig. 7(a)–(c)), viscous relaxation has little impact on swelling at the diffusion time scale. The numerical predictions are close to those that one would have obtained using a diffusion model that neglects viscosity. At the considered simulation times, the mean stress is tensile on the surface, and compressive in the bulk. This stress fully relaxes by creep over time, since there is no elasticity. In contrast, in the initial swelling stages (not shown) the mean stress is first compressive on the surface and tensile in the bulk, due to the larger volume expansion experienced by the swollen outer shell. Concurrently, as more mobile species are inserted into the bulk, the swollen outer layer is pushed away by the inner swelling regions, tending to put the outer shell into tension.

Numerical predictions for $A/\Lambda = 1$ are shown in Fig. 7(d) and (e). When the particle size becomes comparable to the poroviscous length, non-Fickian effects become apparent, giving much flatter concentration profiles at the same normalized diffusion times. In particular, the concentration on the surface markedly deviates from its equilibrium value as set by the external chemical potential. This is primarily due to the kinetics of species insertion, according to which chemical equilibrium is not instantaneously reached locally. The mean stress in the kinetic model also plays a role on the discrepancy between the local free energy and the chemical potential, cf. Eq. (34), however it is negligible in comparison to the bulk viscose relaxation. Also, the mean stress is compressive on the surface at these simulation times, as a result of more prominent viscous effects.

When the particle size is further reduced to $A/\Lambda = 0.1$ (Fig. 7(g)–(i)), profiles of concentration and chemical potential become uniform throughout the particle. The very small composition gradients in turn bring about low stress. The solution obtained with the finite element model then coincides with the solution of the ODE for homogeneous, free mixing:

$$\frac{V_B \dot{C}_B}{\Omega} = \frac{\bar{\mu}_B - F_B}{\beta V_B}. \tag{62}$$

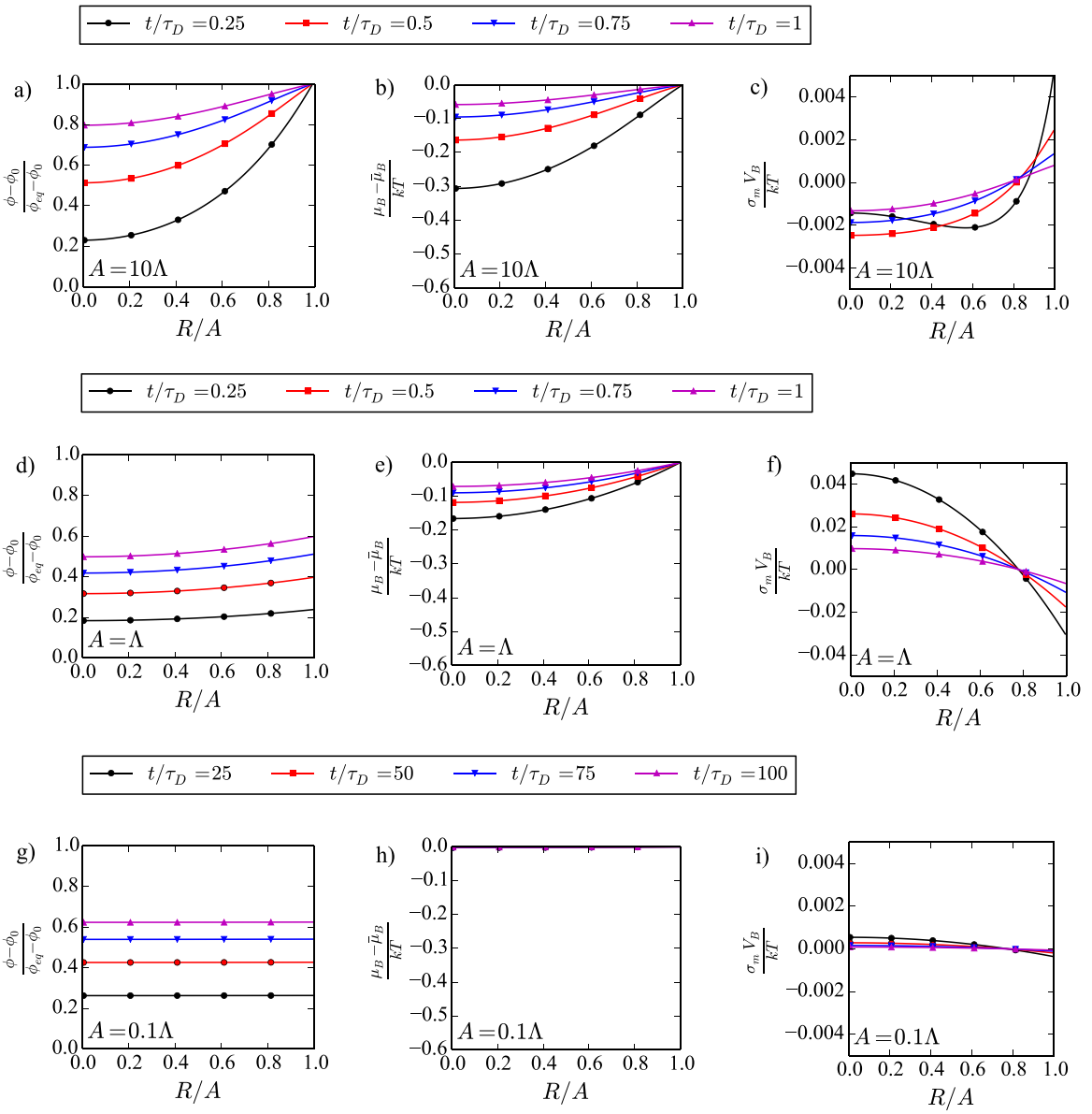

Fig. 7. Profiles of composition, chemical potential and mean stress in swelling particles with different nominal radii: $A = 10\Lambda$ (a–c), $A = \Lambda$ (d–f), and $A = 0.1\Lambda$ (g–i) at different simulation times. In the legend, the time is normalized by the characteristic diffusion time $\tau_D = A^2/D_B$ with $D_B = M_B kT$.

Fig. 8 shows the overall swelling relaxation time as a function of the particle size normalized by the poroviscous length. The overall swelling relaxation time τ_r is here defined as the time needed for the volume fraction at R_0 to reach 99% of the equilibrium value. The relaxation time here is normalized by the material-specific viscous relaxation time $\tau_v = \eta V_B/kT$. The evolution of the swelling relaxation time with particle size is illustrated for different values of the viscosity ratio β/η, including $\beta/\eta = 0$ with non-zero shear viscosity. The dashed line represents the stress-free, swelling response ($\beta = \eta = 0$), for which the relaxation time scales as A^2. When the particle size is large compared to the poroviscous length, all curves collapse onto the diffusion-limited asymptote. When the particle size is small compared to the poroviscous length, all curves corresponding to nonzero bulk viscosity display a plateau corresponding to size-independent, flow-limited swelling. The behavior between these two limits depends on the β/η ratio. In the limit where $\beta = 0$ with $\eta \neq 0$, another diffusion-limited regime is identified for small particle size, with relaxation time slightly smaller than that in the stress-free case $\beta = \eta = 0$. This is attributed to stress-enhanced diffusion stemming from the contribution of mean stress gradient to the driving force for diffusion.

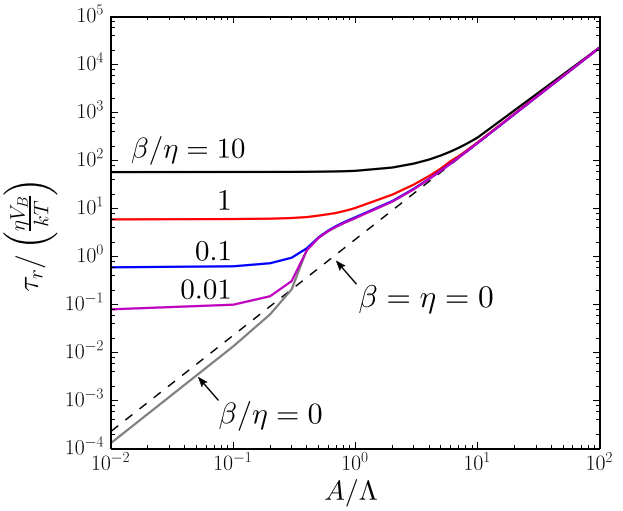

Fig. 8. Swelling relaxation time as a function of the nominal sphere radius for varying values of the bulk-to-shear viscosity ratio β/η. The relaxation time τ_r is normalized by the viscous characteristic time $\tau_v = \eta V_B/kT$, and the radius is normalized by the poroviscous length Λ. The diffusion-limited response when all viscous effects are negligible is also represented (dashed line).

7. Concluding remarks

We have proposed a theory of poroviscosity that couples viscous flow and diffusion in binary solutions. The theory relaxes the classical assumption of local chemical equilibrium. This generalization is motivated by the decoupling between molecular processes for viscous flow and diffusion that may arise in complex liquids and amorphous solids. We have also proposed a Lagrangian, finite element-based approach to solve boundary-value problems. The implications of the theory are discussed in two representative examples. We show that, when the system size is small relative to the material-specific poroviscous length, mixing is limited by species accommodation into the bulk, rather than by diffusion, and the relaxation time becomes size-independent. To focus on the essential ideas, we have neglected elasticity and assumed simple kinetic models of flow. The theory can of course be generalised to account for more elaborated constitutive models. Our theory can be useful to investigate a variety of problems coupling stress and interdiffusion in amorphous systems, such as complex liquids, gels and glasses. It is hoped that experiments can be designed to demonstrate poroviscosity for both flow-limited and diffusion-limited regimes, as well as concurrent shear, dilation, and swap.

Acknowledgment

The work at Harvard was supported by MRSEC (DMR-14-20570).

Appendix A. Eulerian form of the poroviscous theory and comparison with the Navier–Stokes equations

A1. Eulerian form of the poroviscous theory

The poroviscous theory summarised in Section 4 can be written in an equivalent, Eulerian form. Introduce $c_A(\boldsymbol{x}, t)$ and $c_B(\boldsymbol{x}, t)$ the true concentrations of A and B (i.e., the numbers of molecules per unit volume at a point $\boldsymbol{x}$ at time t). The composition variables (8) and (16) write:

$$\xi = \frac{c_B}{c_A + c_B}, \tag{A.1}$$

$$\phi = c_B V_B. \tag{A.2}$$

From the molecular incompressibility conditions (11)–(13) the following relations follow:

$$1 = V_A c_A + V_B c_B, \tag{A.3}$$

$$0 = V_A \frac{\partial c_A}{\partial t} + V_B \frac{\partial c_B}{\partial t}, \tag{A.4}$$

$$0 = c_A \frac{\partial V_A}{\partial t} + c_B \frac{\partial V_B}{\partial t}. \tag{A.5}$$

Describe the overall flow of the solution using the velocity of markers $\boldsymbol{v}(\boldsymbol{x}, t)$, and introduce $\boldsymbol{N}_A$ and $\boldsymbol{N}_B$ the net fluxes of mobile species in the fixed laboratory frame. Diffusion fluxes are defined as the motion of mobile species relative to the marker velocity:

$$\boldsymbol{N}_A = \boldsymbol{j}_A + c_A\boldsymbol{v}, \quad \boldsymbol{N}_B = \boldsymbol{j}_B + c_B\boldsymbol{v}. \tag{A.6}$$

In principle, the velocity of markers, $\boldsymbol{v}$, and the net flux of each species, $\boldsymbol{N}_A$, and $\boldsymbol{N}_B$, can be measured independently in an experiment. Conservation of molecules in the absence of a source term requires that:

$$\frac{Dc_A}{Dt} + c_A div(\boldsymbol{v}) = -div(\boldsymbol{j}_A), \quad \frac{Dc_B}{Dt} + c_B div(\boldsymbol{v}) = -div(\boldsymbol{j}_B), \tag{A.7}$$

where the notation D/Dt refers to the material velocity following the markers:

$$\frac{D(\cdot)}{Dt} = \frac{\partial(\cdot)}{\partial t} + \boldsymbol{v}\cdot grad(\cdot). \tag{A.8}$$

Using (A.3)–(A.5) together with (A.7) leads to an alternative expression of the incompressibility condition:

$$div(\boldsymbol{v}) = tr(\boldsymbol{d}) = -V_A div(\boldsymbol{j}_A) - V_B div(\boldsymbol{j}_B). \tag{A.9}$$

Finally, mechanical equilibrium writes as:

$$grad(\boldsymbol{\sigma}) + \boldsymbol{b} = \boldsymbol{0}, \tag{A.10}$$

where $\boldsymbol{b}$ is the body force.

Eqs. (A.7), (A.9) and (A.10) are 5 PDEs for the 5 primary unknown fields: c_A, c_B and $\boldsymbol{v}$. These PDEs are supplemented by the kinetic models of viscous flow (30), species insertion (31) and (32), and diffusion (35). In the kinetic model of species insertion, the volumetric insertion is expressed in terms of true quantities: $i_A = V_A\frac{Dc_A}{Dt} + c_A V_A d_{kk}$ and $i_B = V_B\frac{Dc_B}{Dt} + c_B V_B d_{kk}$. The mean stress is not prescribed constitutively and may be considered as a field of Lagrange multiplier enforcing the molecular incompressibility condition (A.9).

A2. Comparison with the Navier–Stokes equations for multiple species

One fundamental difference between our poroviscous theory and the standard hydrodynamic equations for multiple species (the Navier–Stokes equations) is the definition of the bulk velocity. The Navier-Stokes equations use the barycentric velocity $\boldsymbol{v}_b$ (the velocity of the center of mass) (de Groot and Mazur, 1984; Landau and Lifshitz, 1987). Alternative definitions of velocity for multiple component flow include the velocity of the center of volume and the velocity of the center of moles (Bird et al., 1960; de Groot and Mazur, 1984; Onsager, 1945). For a description of how the different definitions are related, see Sekerka (2004). All these choices of a reference velocity correspond to a weighted average of the component velocities in the laboratory frame, $\boldsymbol{v}_\alpha = \boldsymbol{N}_\alpha/c_\alpha$. For all such choices, the associated diffusion fluxes are not independent, and diffusion coefficients cannot be prescribed independently. In particular, interdiffusion in a binary solution involves one single mutual diffusion coefficient, whose relationship to the mobility of individual species in the solution is unspecified. In a single species fluid, the standard Navier-Stokes equations do not differentiate flow from self-diffusion (Li et al., 2014). These restrictions do not apply to the present formulation based on marker velocity, in which diffusion fluxes evolve according to independent constitutive relations.

Another direct consequence of the different choice of reference velocity is the form of the incompressibility condition (A.9), which differs from the classical expression $div(\boldsymbol{v}_b) = 0$ of the Navier-Stokes equations. Both theories, however, assume molecular incompressibility. Both also treat the mean stress (or pressure) as a field of Lagrange multipliers to be determined in such a way that the incompressibility condition is satisfied.

There is a well-grounded reason to use the barycentric velocity $\boldsymbol{v}_b$ in the equations of hydrodynamics, for its product with the density, $\rho\boldsymbol{v}_b$, gives the momentum of a unit volume of fluid (Landau and Lifshitz, 1987). It is therefore the natural velocity to use in the inertia term of the momentum conservation equations. In the present work, we assumed quasi-static conditions and therefore neglected the contribution from inertia from the outset, so that this issue was not raised. The classical hydrodynamic theory further relies on the barycentric velocity to write the constitutive equation of Newtonian flow. In a series of papers, Brenner questioned the implicit mono-velocity assumption of classical hydrodynamics (e.g. Brenner, 2005), and proposed an alternative, bi-velocity formulation where the barycentric is used in the momentum balance equations and a volume velocity appears in the constitutive equations (Brenner, 2009). Following Brenner's suggestion, bi-velocity theories were used to analyze the Kirkendall effect (Danielewski and Wierzba, 2009).

Appendix B. Analytical solution to the linearized equations of the 1D interdiffusion problem

Consider the interdiffusion problem in an unbounded binary system in which composition varies only in the x-direction. Similar to Section 6.1, we have that $\sigma_{xx} = 0$ and $d_{yy} = d_{zz} = 0$. In the Eulerian formalism of Appendix A1, the governing equations are the following:

$$\frac{Dc_B}{Dt} + c_B\frac{\partial v}{\partial x} = -\frac{\partial j_B}{\partial x}, \tag{B.1}$$

$$\frac{\partial v}{\partial x} = -V_A \frac{\partial j_A}{\partial x} - V_B \frac{\partial j_B}{\partial x}, \tag{B.2}$$

$$\sigma_m = -\frac{4\eta}{3}\frac{\partial v}{\partial x}. \tag{B.3}$$

Eq. (B.1) expresses the conservation of the molecules of B, Eq. (B.2) enforces molecular incompressibility and Eq. (B.3) is the kinetic model of flow, accounting for the kinematic constraints and mechanical equilibrium. In Eqs. (B.1) and (B.2), the diffusion fluxes are related to the gradients of chemical potentials by the kinetic model (35). Chemical potentials are themselves related to concentration rates by the kinetic model of insertion (31) and (32).

In the following, we follow Stephenson (1988) and solve the set of PDEs (B.1)–(B.3) analytically, assuming small composition and stress perturbation about a reference, equilibrium state. To fix the ideas, let us consider the following initial composition field written as Fourier series:

$$\phi_0(x) = \phi_{eq} + \sum_i \hat{\phi}_{i,0} \exp(iq_i x). \tag{B.4}$$

In Eq. (B.4), ϕ_{eq} is the equilibrium composition of the system, q_i is the wavenumber of the ith Fourier component, and $\hat{\phi}_{i,0} \equiv \hat{\phi}_i(t=0)$ the associated amplitude at time 0. Different from Section 6.1, the initial composition field is thus smooth. We assume that the composition perturbation about the equilibrium state is small, in the sense that $\hat{\phi}_i q_i \ll 1$. For $t>0$, the system relaxes by interdiffusion toward its equilibrium state.

Within the small perturbation approximation, the gradients of composition and stress are proportional to small quantities, and the product of two of these becomes negligible. The velocity of markers is also small, so that the material derivative reduces to the spatial derivative at a fixed position, $D/Dt \approx \partial/\partial t$ (Stephenson, 1988). Eqs (B.1)–(B.3) can be linearized as:

$$\begin{aligned}\frac{\partial \phi}{\partial t} &= kT\Phi(\xi_{eq}M_A + (1-\xi_{eq})M_B)\frac{\partial^2 \phi}{\partial x^2} \\ &+\phi_{eq}(1-\phi_{eq})\left[M_A V_A\left(1+\frac{3\beta_A(1-\phi_{eq})}{4\eta}\right) - M_B V_B\left(1+\frac{3\beta_B\phi_{eq}}{4\eta}\right)\right]\frac{\partial^2 \sigma_m}{\partial x^2} \\ &+\phi_{eq}(1-\phi_{eq})(M_A\beta_A V_A + M_B\beta_B V_B)\frac{\partial}{\partial t}\frac{\partial^2 \phi}{\partial x^2},\end{aligned} \tag{B.5}$$

$$\begin{aligned}&\frac{3\sigma_m}{4\eta} - (M_A V_A(1-\phi_{eq}) + M_B V_B \phi_{eq})\frac{\partial^2 \sigma_m}{\partial x^2} - \frac{3}{4\eta}\left(M_A\beta_A V_A(1-\phi_{eq})^2 + M_B\beta_B V_B \phi_{eq}^2\right)\frac{\partial^2 \sigma_m}{\partial x^2} \\ &= kT\Phi V_m\left(\frac{M_A}{V_B} - \frac{M_B}{V_A}\right)\frac{\partial^2 \phi}{\partial x^2} + (M_A\beta_A V_A(1-\phi_{eq}) - M_B\beta_B V_B\phi_{eq})\frac{\partial}{\partial t}\frac{\partial^2 \phi}{\partial x^2}.\end{aligned} \tag{B.6}$$

In (B.5) and (B.6), the mobility coefficient, viscosity coefficients, partial volumes and mean volume are evaluated at the equilibrium composition (subscript eq omitted for simplicity), as higher order terms in their Taylor expansion about the equilibrium state lead to gradient products that are negligible. The activity coefficient Φ is defined as $\Phi = \partial F_B/\partial \log(\xi)$ and is also evaluated at the equilibrium composition. We look for solutions of the system (B.5) and (B.6) under the form:

$$\phi(x,t) = \phi_{eq} + \sum_i \hat{\phi}_i(t)\exp(iq_i x), \tag{B.7}$$

$$\sigma_m(x,t) = \sum_i \hat{\sigma}_i(t)\exp(iq_i x). \tag{B.8}$$

Thanks to linearity, (B.5) and (B.6) can be solved for each mode amplitude independently. After straightforward (but tedious) calculations, a single ODE for each composition amplitude is obtained:

$$\frac{\partial \hat{\phi}}{\partial t} = -\Gamma(q_i)\hat{\phi}_i(t) = -kT\Phi\bar{M}(q_i)q_i^2\hat{\phi}_i(t). \tag{B.9}$$

The quantity $\Gamma(q_i)$ is the rate constant for the relaxation of mode q_i, and can in turn be expressed in terms of an effective interdiffusion mobility $\bar{M}(q_i)$. The effective mobility is given by:

$$\begin{aligned}\bar{M}(q_i) = &\frac{\frac{3}{4\eta}(\xi_{eq}M_A + (1-\xi_{eq})M_B) + q_i^2 M_A M_B V_m\left(1+\frac{3\beta_A(1-\phi_{eq})^2}{4\eta} + \frac{3\beta_B\phi_{eq}^2}{4\eta}\right)}{\frac{3}{4\eta} + q_i^2\left(M_A V_A(1-\phi_{eq})\left(1+\frac{3\beta_A}{4\eta}\right) + M_B V_B\phi_{eq}\left(1+\frac{3\beta_B}{4\eta}\right)\right)} \\ &+q_i^4(M_A V_A(1-\phi_{eq}))(M_B V_B\phi_{eq})\left(\frac{3\beta_A\beta_B}{4\eta} + \beta_A + \beta_B\right).\end{aligned} \tag{B.10}$$

The relaxation time $\tau_r = 1/\Gamma$ is represented as a function of the wavelength $\lambda = 2\pi/q$ of the perturbation in Fig. 5.

When the kinetics of species insertion is very fast ($\beta_A,\ \beta_B \to 0$), the above analysis is identical to Stephenson's. In the long wavelength limit $(q\Lambda_B)^2 \ll 1$, stress can relax rapidly by viscous flow within the diffusion timescale and Darken's analysis for stress-free system is recovered (Darken, 1948). The net mobility takes the form previously identified by Darken:

$$\bar{M}_D = (1-\xi_{eq})M_B + \xi_{eq}M_A. \tag{B.11}$$

When one species diffuses much faster than the other, say $M_B \gg M_A$, the system relaxation is limited by the diffusion of the fast species, as transport of the slow species occurs essentially by convective transport with the markers.

In the short wavelength limit $(q\Lambda)^2 \gg 1$, and still considering that $\beta_A,\ \beta_B \to 0$, stress relaxation by viscous flow has no time to take place within the diffusion characteristic time. Convective transport plays a negligible role in transporting either species. The incompressibility condition (B.2) then constrains the diffusion fluxes in such a way that mixing proceeds by the swapping of the volume carried by each species. This is achieved through the build-up of a large stress gradient, which effectively accelerates the diffusion of the slow species and slows down the diffusion of the fast species. This regime was called "Nernst-Planck" by Stephenson as it is similar to the interdiffusion of charged species where an electrostatic potential coupled the diffusion fluxes to maintain electroneutrality (Doremus, 1964). The effective mobility in the Nernst-Planck regimes is given by:

$$\bar{M}_{NP} = \frac{M_A M_B V_m}{M_A V_A(1-\phi_{eq}) + M_B V_B \phi_{eq}}. \tag{B.12}$$

When $M_B \gg M_A$, the relaxation process is limited by diffusion of the slow species. Also note that $M_A V_A = M_B V_B$, the Darken and Nernst-Planck expressions of the net mobilities (B.11) and (B.12) are equivalent.

In both the Darken limit and the Nernst-Planck limit, the effective mobility does not depend on the wavenumber. Eq. (B.9) is then equivalent to Fick's second law with a composition-dependent interdiffusion coefficient $\bar{D} = \bar{M}kT\Phi$:

$$\frac{\partial \phi}{\partial t} = \frac{\partial}{\partial x}\left(\bar{D}\frac{\partial \phi}{\partial x}\right). \tag{B.13}$$

When the kinetics of species insertion is not negligible, the asymptotic behavior in the short wavelength limit, $(q\Lambda)^2 \gg 1$, transitions from a Nernst-Planck behavior to a bulk-viscosity limited behavior with net mobility

$$\bar{M}_v(q_i) = \frac{1}{q_i^2}\frac{V_m\left(1+\frac{3\beta_A(1-\phi_{eq})^2}{4\eta}+\frac{3\beta_B\phi_{eq}^2}{4\eta}\right)}{(V_A(1-\phi_{eq}))(V_B\phi_{eq})\left(\frac{3\beta_A\beta_B}{4\eta}+\beta_A+\beta_B\right)}. \tag{B.14}$$

Insertion of (B.14) into (B.9) shows that the rate constant Γ in the bulk flow-limited regime is independent of the wavelength, and that each spatial mode $\hat{\phi}_i$ decays with the same rate constant.

References

Berthier, L., 2011. Dynamic heterogeneity in amorphous materials. Physics 4, 42.
Biot, M.A., 1941. General theory of three-dimensional consolidation. J. Appl. Phys. 12, 155–164.
Bird, R.B., Steward, W.E., Lightfoot, E.N., 1960. Transport Phenomena. John Wiley & Sons.
Bouklas, N., Landis, C.M., Huang, R., 2015. A nonlinear, transient finite element method for coupled solvent diffusion and large deformation of hydrogels. J. Mech. Phys. Solids 79, 21–43.
Brassart, L., Liu, Q., Suo, Z., 2016. Shear, dilation, and swap: mixing in the limit of fast diffusion. J. Mech. Phys. Solids 96, 48–64.
Brassart, L., Suo, Z., 2012. Reactive flow in large-deformation electrodes of lithium-ion batteries. Int. J. Appl. Mech. 4 (3), 1250023.
Brassart, L., Suo, Z., 2013. Reactive flow in solids. J. Mech. Phys. Solids 61, 61–77.
Brassart, L., Zhao, K., Suo, Z., 2013. Cyclic plasticity and shakedown in high-capacity electrodes of lithium-ion batteries. Int. J. Solids Struct. 50, 1120–1129.
Brenner, H., 2005. Navier-Stokes revisited. Physica A 349, 60–132.
Brenner, H., 2009. Bi-velocity hydrodynamics. Physica A 388, 3391–3398.
Camacho, J., Brenner, H., 1995. On convection induced by molecular diffusion. Ind. Eng. Chem. Res. 34, 3326–3335.
Chester, S.A., Anand, L., 2010. A coupled theory of fluid permeation and large deformations for elastomeric materials. J. Mech. Phys. Solids 58, 1879–1906.
Chester, S.A., Di Leo, C.V., Anand, L., 2015. A finite element implementation of a coupled diffusion-deformation theory for elastomeric gels. Int. J. Solids Struct. 52, 1–18.
Coble, R.L., 1963. A model for boundary diffusion controlled creep in polycrystalline materials. J. Appl. Phys. 34, 1679–1682.
Danielewski, M., Wierzba, B., 2009. Diffusion, drift and their interrelation through volume density. Philos. Mag. 89, 331–348.
Darken, L.S., 1948. Diffusion, mobility, and their interrelation through free energy in binary metallic systems. Trans. Am. Inst. Min. Metall. Eng. 175, 184–201.
De Voe, H., 2001. Thermodynamics and Chemistry. Prentice Hall, New-Jersey.
Doremus, R.H., 1964. Exchange and diffusion of ions in glasses. J. Phys. Chem. 68 (8), 2212–2218.
Drozdov, A.D., Christiansen, J., 2013. Stress-strain relations for hydrogels under multiaxial deformation. Int. J. Solids Struct. 50, 3570–3585.
Ediger, M.D., 2000. Spatially heterogeneous dynamics in supercooled liquids. Ann. Rev. Phys. Chem. 51, 99–128.
Edward, J.T., 1970. Molecular volumes and the Stokes-Einstein relation. J. Chem. Educ. 47, 261–270.
Einstein, A., 1905. Ber die von der molekularkinetischen theorie der wrme geforderte bewegung von in ruhenden flssigkeiten suspendierten teilchen [on the movement of small particles suspended in a stationary liquid demanded by the molecular-kinetic theory of heat]. Annalen der Physik 17, 549–560.
Fischer, F.D., Svoboda, J., 2014. Diffusion of elements and vacancies in multi-component systems. Prog. Mater. Sci. 60, 338–367.
Flory, P.J., 1942. Thermodynamics of high polymer solutions. J. Chem. Phys. 10, 51–61.
de Groot, S.R., Mazur, P., 1984. Non-Equilibrium Thermodynamics, 2nd Ed.. North-Holland.
Gurtin, M.E., Fried, E., Anand, L., 2010. The Mechanics and Thermodynamics of Continua. Cambridge University Press, Cambridge.
Herring, C., 1950. Diffusional viscosity of a polycrystalline solid. J. Appl. Phys. 21, 437–445.
Hong, W., Zhao, X., Zhou, J., Suo, Z., 2008. A theory of coupled diffusion and large deformation in polymeric gels. J. Mech. Phys. Solids 56, 1779–1793.
Hu, Y., Suo, Z., 2012. Viscoelasticity and poroelasticity in elastomeric gels. Acta Mech. Solida Sinica 25, 2012.

Karmakar, S., Dasgupta, C., Sastry, S., 2014. Growing length scales their relation to timescales in glass-forming liquids. Ann. Rev. Condens. Matter Phys. 5, 255–284.
Landau, L.D., Lifshitz, E.M., 1987. Fluid Mechanics, 2nd Ed. Butterworth-Heinemann.
Larché, F.C., Cahn, J.W., 1985. The interactions of composition and stress in crystalline solids. Acta Metall. 33 (3), 331–357.
Li, J., Liu, Q., Brassart, L., Suo, Z., 2014. Mechanics of supercooled liquids. J. Appl. Mech. 81, 111007.
Liu, Q., Huang, S., Suo, Z., 2015. Brownian motion of molecular probes in supercooled liquids. Phys. Rev. Lett. 114 (22), 224301.
Mandel, J., 1966. Cours de mécanique des milieux continus. Gauthier-Villars.
Mishin, Y., Warren, J.A., Sekerka, R.F., Boettinger, W.J., 2013. Irreversible thermodynamics of creep in crystalline solids. Phys. Rev. B 88, 184303.
Onsager, L., 1945. Theories and problems of liquid diffusion. Ann. N. Y. Acad. Sci. 46 (5), 241–265.
Pharr, M., Zhao, K., Suo, Z., Ouyang, F.-Y., Liu, P., 2011. Concurrent electromigration and creep in lead-free solder. J. Appl. Phys. 110, 083716.
Phillips, R.J., Deen, W.M., Brady, J.F., 1989. Hindered transport of spherical macromolecules in fibrous membranes and gels. AIChE J. 35 (11), 1761–1769.
Sekerka, R.F., 2004. Similarity solutions for a binary diffusion couple with diffusivity and density dependent on composition. Prog. Mater. Sci. 49, 511–536.
Stephenson, G.B., 1988. Deformation during interdiffusion. Acta Metall. 36, 2663–2683.
Suo, Z., 2004. A continuum theory that couples creep and self-diffusion. J. Appl. Mech. 71, 646–651.
Villani, A., Busso, E.P., Forest, S., 2015. Field theory and diffusion creep predictions in polycrystalline aggregates. Model. Simul. Mater. Sci. Eng. 23, 055006.
Zhao, K., Pharr, M., Cai, S., Vlassak, J., Suo, Z., 2011. Large plastic deformation in high-capacity lithium-ion batteries caused by charge and discharge. J. Am. Ceram. Soc. 94, 226–235.